

# Permeability and Inertia Coefficient of Wire-Mesh Porous Media Estimated by a Darcy-Forchheimer Equation



Suradech Sinjapo, Panuwat Chanmak, and Bundit Krittacom

**Abstract** The airflow through the wire-mesh screen inside the circular pipe was experimented with to investigate the permeability ( $K$ ) and the inertia coefficient ( $F$ ) based on Darcy–Forchheimer’s principle. Five pores per inch (PPI) of the SUS304 stainless wire-mesh (i.e., 6, 8, 10, 12, and 14) were examined with the wire diameter ( $d_w$ ) that was kept at 0.36 mm. From such PPIs, the porosity ( $\varepsilon$ ) yielded 0.866, 0.822, 0.777, 0.733, and 0.688, respectively. Five different stacked thicknesses ( $H$ ) were conducted in the range of 1.44–7.20 mm. The linear formulation adapted from the Darcy–Forchheimer equation was employed, with  $\Delta P = a + bu$  denoting the relationship between pressure drop ( $\Delta P$ ) and velocity ( $u$ ). The  $\Delta P$  was measured using a digital manometer by changing  $u$  between 0.262 and 1.833 m/s. The experiment revealed that when  $\varepsilon$  rose,  $K$  grew and  $F$  dropped. With the impact of  $H$ , the opposite situation was obtained— $K$  dropped and  $F$  rose. The correlations of  $K$  and  $F$  were proposed by  $K = (1.3425 + 6.2161\varepsilon - 0.4977H) \times 10 - 7$  and  $F = 0.6296 - 0.7524\varepsilon + 0.0653H$ . To validate the proposed correlations, two available models, consisting of the equation of Gebart and Koponen, were examined

---

S. Sinjapo

Development in Technology of Porous Materials Research Laboratory (DiTo-Lab),  
Rajamangala University of Technology Isan, Nakhonratchasima, Thailand

Department of Railway System Engineering, Faculty of Engineering and Architecture,  
Rajamangala University of Technology Isan, Nakhonratchasima, Thailand

P. Chanmak

Development in Technology of Porous Materials Research Laboratory (DiTo-Lab),  
Rajamangala University of Technology Isan, Nakhonratchasima, Thailand

Department of Mechanical Engineering, Faculty of Industrial Education, Rajamangala  
University of Technology Suvarnabhumi, Nonthaburi, Thailand

B. Krittacom (✉)

Development in Technology of Porous Materials Research Laboratory (DiTo-Lab),  
Rajamangala University of Technology Isan, Nakhonratchasima, Thailand

Department of Mechanical Engineering, Faculty of Engineering and Architecture, Rajamangala  
University of Technology Isan, Nakhonratchasima, Thailand

e-mail: [bundit.kr@rmuti.ac.th](mailto:bundit.kr@rmuti.ac.th)

for  $K$ , and Du Plessis's equation was adopted for  $F$ . In comparison, a favorable agreement was reached. As a result, the proposed models were very credible and straightforward to apply.

**Keywords** Permeability · Darcy–Forchheimer equation · Wire-mesh porous media

## 1 Introduction

The fluid flow in porous media has received considerable attention because of its importance in the areas of pneumatic–hydraulic applications [1]. The principle of fluid transport within porous media is used in many works—for example, petroleum technology [2, 3], groundwater hydrology [4, 5], micromachining work [6, 7], and fuel cells [8]. For fluid moving at a sufficiently high velocity through porous media, the pressure drop ( $\Delta P$ ) versus flow velocity is given by the Forchheimer equation [9]:

$$\Delta P = \left(\frac{\mu L_0}{K}\right)u + \left(\frac{\rho FL_0}{\sqrt{K}}\right)u^2 \quad (1)$$

where  $\mu$ ,  $\rho$ ,  $L_0$ ,  $K$ , and  $F$  are fluid viscosity, fluid density, testing length, permeability, and inertia coefficient (or Ergun coefficient) [10], respectively. The Forchheimer equation (Eq. 1) modified from the Darcy law [11] has, generally, two terms expressing the viscous and the inertial effects, respectively.

Permeability ( $K$ ) and the inertia coefficient ( $F$ ) estimated from the Forchheimer equation are the key to the transmitted ability of structure. For macroscopic phenomena of fluid flow through the porous matrix, the quantity of  $K$  and  $F$  have perhaps the most important property to describe and to thoroughly understand the flow phenomena. Traditionally, the void structure in a porous matrix, as defined by the porosity ( $\varepsilon$ ), becomes complex, resulting in a convoluted flow pattern inside and across the void [12].

The Kozeny–Carman equation [13, 14] was the most classical equation explained in the relationship between  $K$  and porosity ( $\varepsilon$ ). The measurement of  $K$  and  $F$  for the foam and fibrous structure were conducted by many works [15–17]. In addition, several experimental investigations and numerous numerical analytical details using the lattice Boltzmann technique [18–20] have been undertaken during the previous few decades. Gebart [21] investigated  $K$  with a combination method of theoretical, numerical, and experimental studies for which he proposed the functional form of  $K$  to  $\varepsilon$  (porosity). A good application of his function was obtained for  $\varepsilon \geq 0.65$ . Du Plessis et al. [22] presented a correlation for predicting the  $F$ . This equation gave good application in the high porosity range. Koponen et al. [23] applied the lattice Boltzmann method to establish an empirical relationship of  $K$  for  $\varepsilon$  in the range of  $0.4 \leq \varepsilon \leq 0.95$ .

Recently, the corresponding author and coworker performed experimentally to measure the  $K$  of the stainless wire-mesh screen with the porosity range of 0.794–0.943 [24]. The SUS304 stainless wire-mesh screen was tested at four different pores per inch (PPI) (i.e., 4, 8, 10, and 12). The wire diameter did not use the same size. A correlation of  $K$  was only proposed but  $F$  was not discussed.

Based on previous work [24], this chapter wants to extend the boundary of the investigation. Two PPIs (6 and 14) were added experimentally, but PPI = 4 did not change because the enhancement performance was insignificant [25, 26]. The wire diameter ( $d_w$ ) was used with the size kept at 0.36 mm. Thus, five PPIs of the SUS304 stainless wire-mesh (i.e., 6, 8, 10, 12, and 14) were tested by which the porosity ( $\epsilon$ ) became 0.866, 0.822, 0.777, 0.733, and 0.688, respectively. The wire-mesh screen was prepared as six stacked wire-mesh bundles for which a distance between two adjacent stacked wire-meshes ( $L$ ) was 80 mm. The stacked thicknesses ( $H$ ) of wire-mesh porous media organized with five  $H$ s was: 1.44, 2.88, 4.32, 5.76, and 7.20 mm. Finally, two correlations of  $K$  and  $F$  on  $\epsilon$  and  $H$  were reported, and the comparison results of a present correlation with available functions were discussed.

## Nomenclature

The following nomenclature is used in this chapter:

$a$	Slope of the line
$b$	y-axis ( $\Delta P/u$ ) intercept
$d_w$	Wire diameter, m
$F$	Inertia coefficient
$H$	Porous thickness, m
$K$	Permeability, $m^2$
$L_0$	Testing length, m
PPI	Pores per inch
$Q$	Volumetric flow rate, $m^3/s$
$r$	Material diameter, m
$R^2$	Determination coefficient
$T_{in}$	Inlet air temperature, $^{\circ}C$
$u$	Fluid velocity, m/s
$\Delta P$	Pressure drop across testing pipe, $N/m^2$
$\epsilon$	porosity
$\rho$	Fluid density, $kg/m^3$
$\mu$	Fluid viscosity, Pa-s

## 2 Experimental Setup

### 2.1 Experimental Diagram

Figure 13.1 shows a schematic diagram of the experiment to evaluate the permeability ( $K$ ) and the inertia coefficient ( $F$ ) of wire-mesh porous media attached inside the circular pipe based on the same experimental system of Huchaiyaphum et al.

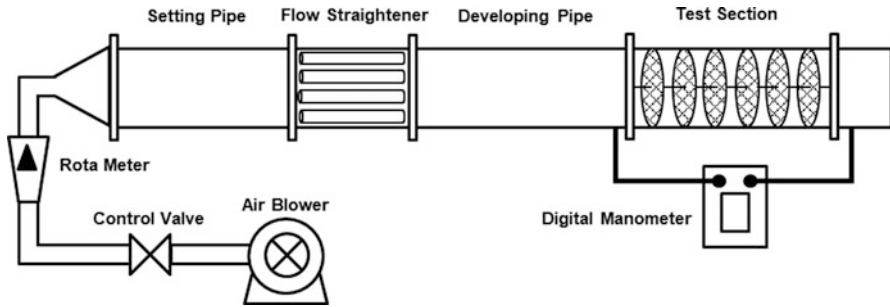


Fig. 13.1 Schematic diagram of the experimental setup [24]

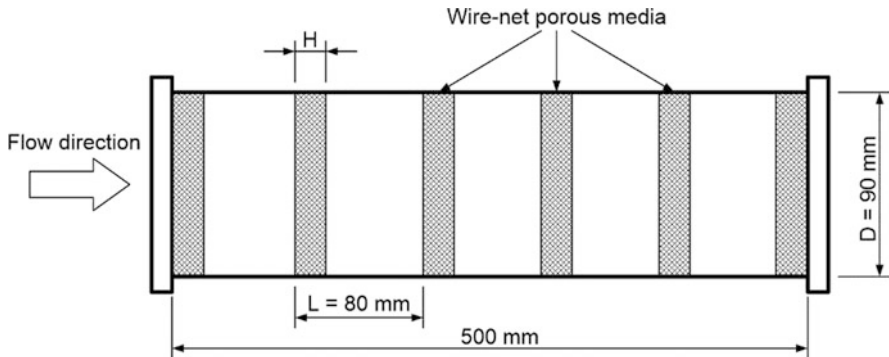


Fig. 13.2 A testing pipe with the installation of wire-mesh porous media [24]

[24]. This test rig is a good general way for monitoring the pressure drop ( $P$ ) through the pipe because it is a straightforward procedure for determining  $K$  and  $F$  [27, 28].

To understand in the test section, a testing pipe made of SUS304 stainless steel with an inner diameter of 90 mm and a length of 500 mm is presented by Fig. 13.2, which is like that of Ref. [24]. The stainless wire-mesh screen with a diameter ( $d_w$ ) of 0.36 mm was employed as porous media, and it was provided as six bundles to attach inside the pipe. The distance between two adjacent porous bundles ( $L$ ) was kept at 80 mm. In the experiment, there were two interesting parameters: porosity ( $\epsilon$ ) converted from PPI, and porous thickness ( $H$ ). Table 13.1 summarizes the 25 cases, constructed from five  $\epsilon$  and five  $H$ , for measuring the pressure drop ( $\Delta P$ ) and evaluating  $K$  and  $F$ .

As shown in Fig. 13.1, an experimental procedure was the same as in a previous work [24]. To get the understanding again, however, the experimental procedure was represented. In the beginning, the fresh air at the ambient condition (i.e., inlet air temperature,  $T_{in}$ , of 27 °C) was supplied by an air blower into the system. Then, the airflow rate ( $Q$ ) controlled with a valve was monitored by Rotameter.

The  $Q$  was changing at the range of 0.00167 m<sup>3</sup>/s (100 LPM)–0.01167 m<sup>3</sup>/s (700 LPM). The fresh air flowed past the setting pipe to provide a uniform streamline

**Table 13.1** Testing cases of wire-mesh porous media

Case	PPI	Porosity ( $\epsilon$ )	$H$ (mm)
1	6	0.866	1.44 (4 screen)
2	6	0.866	2.88 (8 screen)
3	6	0.866	4.32 (12 screen)
4	6	0.866	5.76 (16 screen)
5	6	0.866	7.20 (20 screen)
6	8	0.822	1.44 (4 screen)
7	8	0.822	2.88 (8 screen)
8	8	0.822	4.32 (12 screen)
9	8	0.822	5.76 (16 screen)
10	8	0.822	7.20 (20 screen)
11	10	0.777	1.44 (4 screen)
12	10	0.777	2.88 (8 screen)
13	10	0.777	4.32 (12 screen)
14	10	0.777	5.76 (16 screen)
15	10	0.777	7.20 (20 screen)
16	12	0.733	1.44 (4 screen)
17	12	0.733	2.88 (8 screen)
18	12	0.733	4.32 (12 screen)
19	12	0.733	5.76 (16 screen)
20	12	0.733	7.20 (20 screen)
21	14	0.688	1.44 (4 screen)
22	14	0.688	2.88 (8 screen)
23	14	0.688	4.32 (12 screen)
24	14	0.688	5.76 (16 screen)
25	14	0.688	7.20 (20 screen)

and the uniform flow of air was completely obtained while passing the straightened pipe. In addition, to generate the full developing flow in a pipe, its length of 900 mm (10D) [29] was aligned horizontally in front of a testing pipe. Finally, the pressure drop ( $\Delta P$ ) across the testing pipe was measured by a digital manometer with an accuracy of  $\pm 0.3\%$ .

### 2.2 *Estimated Equation of Permeability (K) and Inertia Coefficient (F)*

In evaluation of permeability ( $K$ ) from the data accumulated by the experimental procedure, the Forcheimer equation [9] or Eq. (1) can be calculated by:

$$\Delta P = au + bu^2 \tag{2}$$

$$a = \frac{\mu L_0}{K} \quad (3)$$

$$b = \frac{\rho F L_0}{\sqrt{K}} \quad (4)$$

Here,  $u$  is air velocity with the range of 0.262 m/s–1.833 m/s, which is calculated by  $u = Q/A$  ( $A$  is the cross-section area of a testing pipe). For the value of  $L_0$ ,  $H$  is applied.

Based on Ref. [24], Eq. (2) was transformed into a linear equation as follows:

$$\frac{\Delta P}{u} = a + bu \quad (5)$$

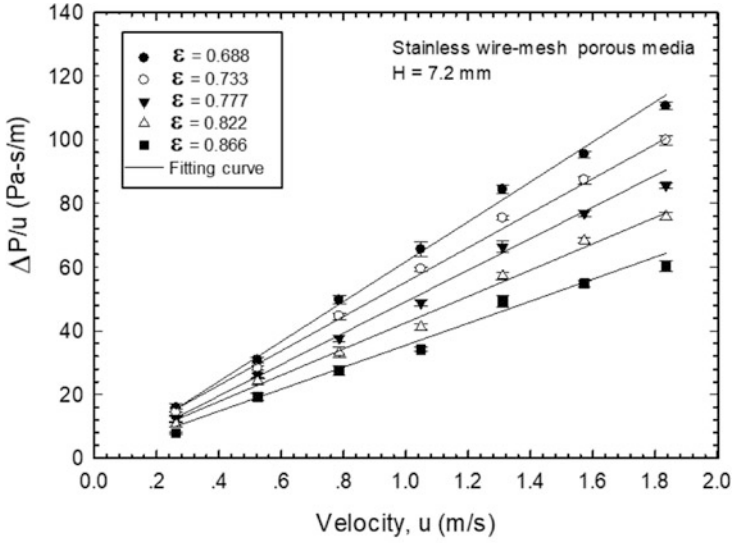
where variable  $a$  is the slope of the line and  $b$  is the  $y$ -axis ( $\Delta P/u$ ) intercept. Eq. (5) was fitted by the linear regression method [30]. Such two variables ( $a$  and  $b$ ) were easiest to be obtained. Thus, after  $K$  was estimated by  $\mu L_0/a$ ,  $F$  was automatically given by  $bK^{1/2}/\rho L_0$ .

### 3 Results and Discussion

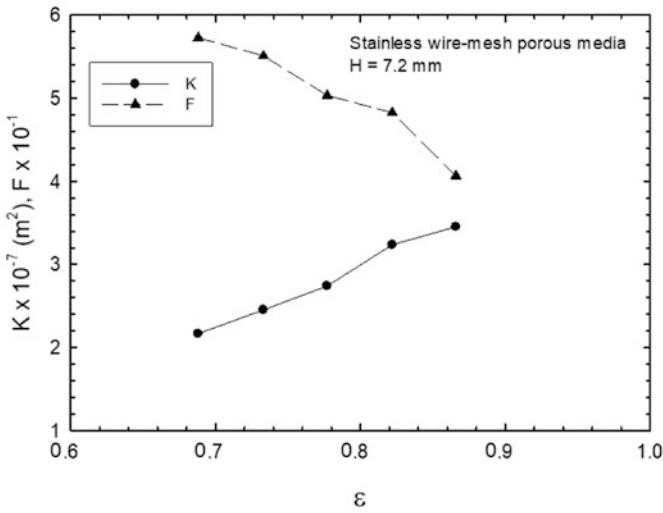
#### 3.1 Effect of $\varepsilon$ on $K$ and $F$

Figure 13.3a presents the relationship between the ratio of pressure drop to air velocity ( $\Delta P/u$ ), and air velocity ( $u$ ) for the effect of porosity ( $\varepsilon$ ) at the experimental condition of porous thickness ( $H$ ) of 7.2 mm. From the experiment, it was found that the  $\Delta P/u$  was increased as rising  $u$  owing to the nature of fluid flow in the pipe [24, 31, 32]. As a constant of  $u$ , the pressure drop ( $\Delta P/u$ ) was reduced as increasing  $\varepsilon$  (PPI reduce) because of the difficult flow that occurred at a lower porosity ( $\varepsilon$ ) [32–35]. In the figure, the solid lines indicate the fitted curves across the experimental points (symbols) based on regression analysis. The coefficients of determination ( $R^2$ ) between the solid line and the symbols were all more than 0.98, indicating that this regression was credible [30].

In Table 13.2, the solid lines (linear equations) are summarized. The coefficients  $a$  and  $b$  specified in Eq. (5) may be found by fitting a linear equation across these points. By substituting the  $a$  and  $b$  from this figure into Eqs. (5) and (6), the  $K$  and the  $F$  were obtained. The relationship of  $K$  and  $F$  on  $\varepsilon$  at the  $H = 7.2$  mm is illustrated in Fig. 13.3b. As  $\varepsilon$  increased, the  $K$  was decreased but the  $F$  grew. This was described by the effect of a raiser pressure drop ( $\Delta P$ ) similar with the result in Fig. 13.3a. The trend of  $K$  and  $F$  of the present study was consistent to the available works [28, 36, 37].



(a) relation between  $\Delta P/u$  and  $u$



(b) relation of  $K$  and  $F$  on  $\epsilon$

**Fig. 13.3** Effect of  $\epsilon$  on  $\Delta P/u$ ,  $K$  and  $F$ . (a) Relationship between  $\Delta P/u$  and  $u$ . (b) Relationship of  $K$  and  $F$  on  $\epsilon$

**Table 13.2** Linear equation of  $\Delta P/u$  for effect of  $\varepsilon$ 

Porosity ( $\varepsilon$ )	Linear equation	$R^2$
0.866 (PPI = 6)	$\Delta P/u = 0.386 + 34.142u$	0.986
0.822 (PPI = 8)	$\Delta P/u = 0.411 + 41.996u$	0.993
0.777 (PPI = 10)	$\Delta P/u = 0.486 + 47.439u$	0.995
0.733 (PPI = 12)	$\Delta P/u = 0.543 + 55.252u$	0.997
0.688 (PPI = 14)	$\Delta P/u = 0.614 + 61.086u$	0.996

### 3.2 Effect of H on K and F

Figure 13.4a presents the relationship between the  $\Delta P/u$  and  $u$  at the porosity ( $\varepsilon$ ) of 0.688 (PPI = 14) for the effect of porous thickness ( $H$ ). The  $\Delta P/u$  was increased with  $u$ , which was the same trend in effect for  $\varepsilon$  (see Fig. 13.3a). For constant of  $u$ , the trend of pressure drop ( $\Delta P/u$ ) was raised as increasing  $H$  because it was the effect of a thicker porous media, resulting in a more difficult flow of air through the porous media had occurred [24, 31, 32].

In considering the fitting curves, the solid lines gave good agreement to the experiments (symbols). The determination coefficients ( $R^2$ ) of the developed equations became higher than 0.96, and they were summarized in Table 13.3. Figure 13.4b illustrates the relationship between the  $K$  and the  $F$  on the impact of  $H$ . As  $H$  increases, the trend of  $K$  was decreased, but the  $F$  was rose. This can be explained by the same reason shown in Fig. 13.4a.

### 3.3 Regression Analysis of K and F to $\varepsilon$ and H

From the 25 cases of the present experiment based on the range of  $0.733 \leq \varepsilon \leq 0.866$  and  $1.44 \leq H \leq 7.20$  mm, two equations of  $K$  and  $F$  generated by the multiregression method are given as follows:

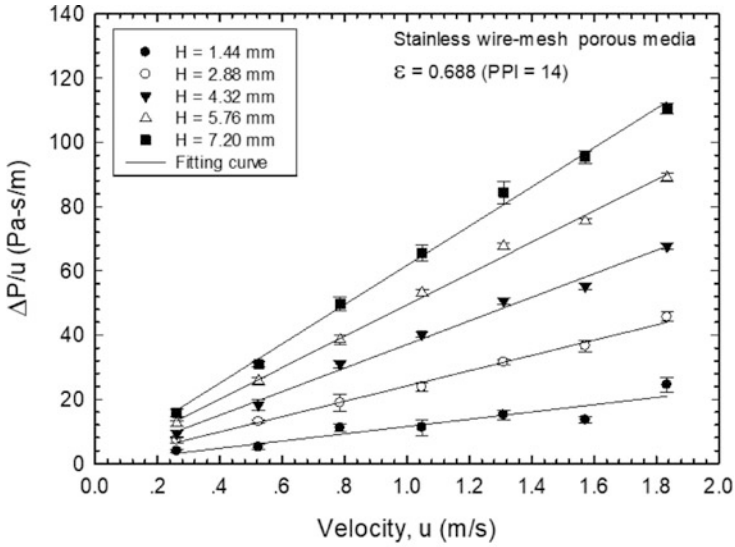
$$K = (1.3425 + 6.2161\varepsilon - 0.4977H) \times 10^{-7} \quad (6)$$

$$F = 0.6296 - 0.7524\varepsilon + 0.0653H \quad (7)$$

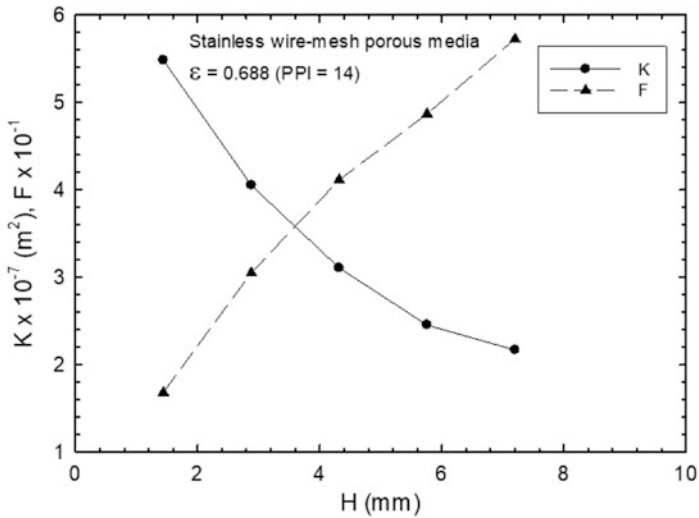
To validate both equations, the comparison results of equations (Eqs. (6) and (7)) to available empirical equations are reported by Fig. 13.5. The equation proposed by Gebart [21] and Koponen et al. [23] were employed to validate the  $K$  (see Fig. 13.5a), while the validation of  $F$  was compared with Du Plessis's equation alone (see Fig. 13.5b) [22].

As seen in Fig. 13.5a, the solutions from the present equation of  $K$  at the  $H = 7.20$  mm gave good agreement with both available works [21, 23]. For





(a) relation between  $\Delta P/u$  and  $u$



(b) relation of  $K$  and  $F$  on  $H$

**Fig. 13.4** Effect of  $H$  on  $\Delta P/u$ ,  $K$  and  $F$ . (a) Relationship between  $\Delta P/u$  and  $u$ . (b) Relationship of  $K$  and  $F$  on  $H$

**Table 13.3** Linear equation of  $\Delta P/u$  for effect of  $H$ 

Porous thickness ( $H$ )	Linear equation	$R^2$
1.44 mm (4 screen)	$\Delta P/u = 0.243 + 11.288u$	0.965
2.88 mm (8 screen)	$\Delta P/u = 0.328 + 23.802u$	0.994
4.32 mm (12 screen)	$\Delta P/u = 0.428 + 36.657u$	0.992
5.76 mm (16 screen)	$\Delta P/u = 0.543 + 48.838u$	0.996
7.20 mm (20 screen)	$\Delta P/u = 0.614 + 64.086u$	0.996

comparison of  $F$  at  $H = 7.20$  mm, as shown in Fig. 13.5b, the same trend of the previous equation and Du Plessis' s model [22] was achieved. A higher level from that equation, however, appeared. Thus, it can be said that the accuracy of the proposed correlation was practical use in the examined range.

## 4 Conclusion

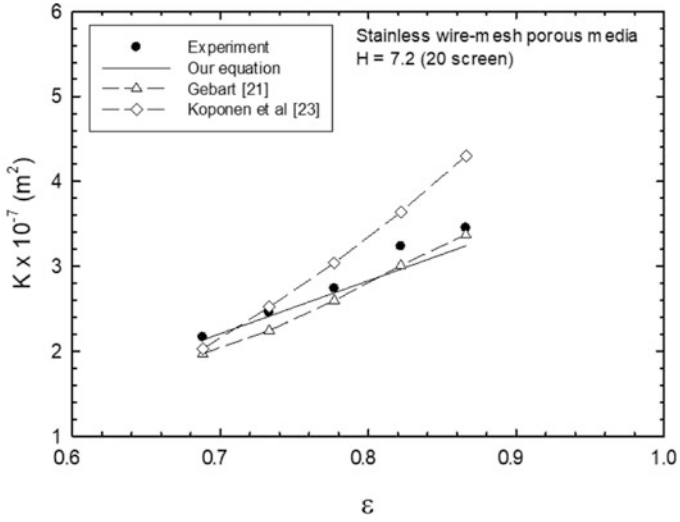
An experimental and analytical study investigating the permeability ( $K$ ) and the inertia coefficient ( $F$ ) of wire-mesh porous media, based on Forchheimer principle, was proposed. Stainless SUS304 with different porosity ( $\epsilon$  or PPI) and thicknesses ( $H$ ) were examined. The trend of  $K$  increased and  $F$  decreased when  $\epsilon$  was raised. The opposite result was obtained by increasing  $H$ :  $K$  decreased and  $F$  increased. From the fitting process, equation of  $K$  and  $F$ , estimated by multi-regression method, can be shown by

$$K = (1.3425 + 6.2161\epsilon - 0.4977H) \times 10^{-7} \text{ and}$$

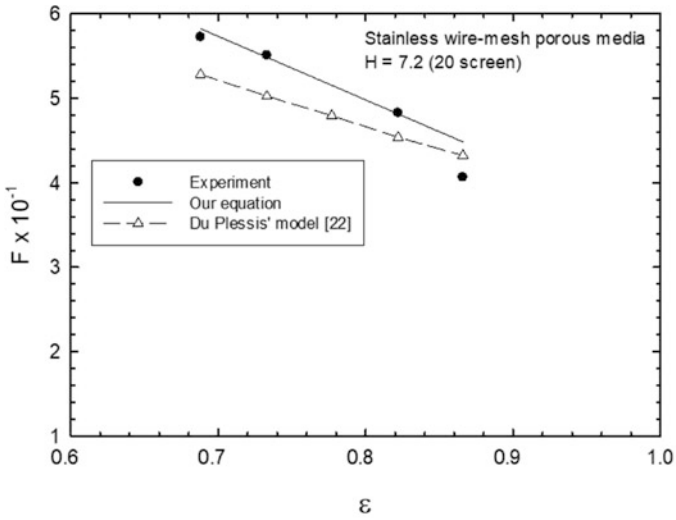
$$F = 0.6296 - 0.7524\epsilon + 0.0653H$$

For which the accuracy was in the range of  $0.733 \leq \epsilon \leq 0.866$  and  $1.44 \leq H \leq 7.20$  mm. Good agreement between this chapter's equations and other available works [21–23] was obtained.

**Acknowledgments** The authors sincerely appreciate the finance support from Faculty of Engineering and Architecture, Rajamangala University of Technology Isan (RMUTI) for the registration fee. Thanks also to Mr. Bunpot Boorana, Mr. Kittichai Muangkoed, and Mr. Julladid Suksabai, undergraduate students of the Mechanical Engineering Department, for recording the experimental data.



(a) relation between  $K$  and  $\epsilon$



(b) relation between  $F$  and  $\epsilon$

**Fig. 13.5** Comparison of  $K$  and  $F$  between the present equation with available works. (a) Relationship between  $K$  and  $\epsilon$ . (b) Relationship between  $F$  and  $\epsilon$

## References

1. M.E. Beygi, F. Rashidi, Analytical solutions to gas flow problems in low permeability porous media. *Transp. Porous Media* **87**, 421–436 (2011)
2. K. Arash, H.M. Mehdi, A.R. Deresh, Reliable method for the determination of surfactant retention in porous media during chemical flooding oil recovery. *Fuel* **158**, 122–128 (2015)
3. A. Telmadrreie, D. Ankit, J.T. Japan, K. Ergun, C. Phillip, CO<sub>2</sub> microbubbles-a potential fluid for enhanced oil recovery: Bulk and media studies. *J. Pet. Sci. Eng.* **138**, 160–173 (2016)
4. D. Bernard, W.M. John, Groundwater age in fractured porous media: Analytical solution for parallel fractures. *Adv. Water Resour.* **37**, 127–135 (2012)
5. F. Alessio, S. Anna, A numerical method for two-phase flow in fractured porous media with non-matching grids. *Adv. Water Resour.* **62**, 454–464 (2013)
6. F. Ali, L. Faical, Two-phase flow hydrodynamic study in micro-packed beds – Effect of bed geometry and particle size. *Chem. Eng. Process.* **78**, 27–36 (2014)
7. T.F. Zhao, C.Q. Chen, The shear properties and deformation mechanisms of porous metal fiber sintered sheets. *Mech. Mater.* **70**, 33–40 (2014)
8. K.N. Kim, J.H. Kang, S.G. Lee, J.H. Nam, C.J. Kim, Lattice Boltzmann simulation of liquid water transport in microporous and gas diffusion layers of polymer electrolyte membrane fuel cells. *J. Power Sources* **278**, 703–717 (2015)
9. P. Forchheimer, Wasserbewegung durch boden. *VDI Z.* **45**, 1782–1788 (1901)
10. S. Ergun, Fluid flow through packed column. *Chem. Eng. Sci.* **48**, 89–94 (1952)
11. H. Darcy, *Les Fontaines Publiques de la ville de Dijon* (Dalmont, Paris, France, 1856)
12. A. Nabovati, E.W. Llewellyn, C.M. Antonio, A general model for the permeability of fibrous porous media based on fluid flow simulations using the lattice Boltzmann method. *Compos. Part A* **40**, 860–869 (2009)
13. J. Kozeny, Ueber kapillare Leitung des Wassers in Boden. *Stizungsber Akad Wiss Wien.* **136**, 271–306 (1927)
14. P.C. Carman, Permeability of saturated sands, soils and clays. *J. Agric. Sci.* **18**, 262–273 (1939)
15. K. Vafai, C.L. Tien, Boundary and inertia effects on convective mass transfer in porous media. *Int. J. Heat Mass Transf.* **25**(8), 1183–1190 (1982)
16. Joseph, D.A. Nield, G. Papanicolaou, Nonlinear equation governing flow in a saturated porous medium. *Water Resour. Res.* **18**, 1049–1052 (1982)
17. B. Antohe, J.L. Lage, D.C. Price, R.M. Weber, Experimental determination of permeability and inertial coefficient of mechanically compressed aluminium metal layers. *ASME J. Fluids Eng.* **119**, 404–412 (1997)
18. M.D. Aminu, B.U. Ardo, A novel approach for determining permeability in porous media. *J. Pet. Environ. Biotechnol.* **6**, 1–5 (1994)
19. A. Eshghinejadfard, L. Daroczy, G. Janiga, D. Thevenin, Calculation of the permeability in porous media using the lattice Boltzmann method. *Int. J. Heat Fluid Flow* **62**, 93–103 (2016)
20. P. Yang, Z. Wen, R. Duo, X. Lui, Permeability in multi-size structures of random packed porous media using three-dimensional lattice Boltzmann method. *Int. J. Heat Mass Transf.* **106**, 1368–1375 (2017)
21. B.R. Gebart, Permeability of unidirectional reinforcements for RTM. *J. Compos. Mater.* **26**(8), 1100–1133 (1992)
22. P. Du Plessis, A. Montillet, J. Comiti, J. Legrand, Pressure drop prediction for flow through high porosity metallic foam. *Chem. Eng. Sci.* **49**, 3545–3553 (1994)
23. A. Koponen, D. Kandhai, E. Hellen, Permeability of three-dimensional random fiber webs. *Phys. Rev. Lett.* **80**, 716–719 (1998)
24. N. Huchaiyaphum, S. Panpanya, B. Krittacom, Permeability of wire-net porous media determined by a simple Darcy-Forchheimer equation. *J. Res. Appl. Mech. Eng.* **6**(1), 63–71 (2018)

25. P. Waramit, P. Chanmak, R. Peamsuwan, B. Krittacom, Forced convection enhancement of air flowing inside circular pipe with varying the pitch (P) of wire-mesh porous media. *Energy Rep.* **7**(sup. 5), 70–82 (2021)
26. B. Krittacom, and A. Klamnoi: A simplified linear scattering phase function for solving equation of radiative heat transfer, presented in Proceedings of the 4th International Symposium on Engineering, Energy and Environments, Pattaya, Thailand, November 8–10 (2015), pp. 457–463.
27. A.A. Mohamad, Heat transfer enhancements in heat exchangers fitted with porous media part I: Constant wall temperature. *Int. J. Therm. Sci.* **42**(4), 385–395 (2003)
28. B.I. Pavel, A.A. Mohamad, An experimental and numerical study on heat transfer enhancement for gas heat exchangers fitted with porous media. *Int. J. Heat Mass Transf.* **47**(23), 4939–4952 (2004)
29. Y.A. Cengel, A.F. Ghajar, *Heat and Mass Transfer: Fundamental and Applications*, 4th edn.9 (McGraw-Hill Inc., Singapore, 2011)
30. W. Cheney, D. Kincaid, *Numerical Mathematics and Computing*, 7th edn. (Brooks/Cole, Cengage Learning, Boston, USA, (2013)
31. L. Green Jr., Fluid flow through porous metals. *J. Appl. Mech.* **18**, 39–45 (1951)
32. M. Kaiany, *Principle of Heat Transfer in Porous Media*, 2nd edn. (Springer-Verlag, New York, 1996)
33. B. Krittacom, P. Amatachaya, R. Sangchot, Energy balance in Al-Co open-celled foam of transpiration cooling. *Appl. Mech. Mater.* **575**, 41–45 (2014)
34. P. Amatachaya, B. Krittacom, Combustion mechanism of gas porous burner installed an in-line tube-bank heat exchanger. *Energy Procedia* **138**, 50–55 (2017)
35. P. Waramit, P. Chanmak, R. Peamsuwan, B. Krittacom, Forced convection enhancement of air flowing inside circular pipe with varying the pitch (P) of wire-mesh porous media. *Energy Rep.* **7**(Supple 5), 70–82 (2021)
36. A. Bhattacharya, V.V. Calmidi, R.L. Mahajan, Thermophysical properties of high porosity metal foam. *Int. J. Heat Mass Transf.* **45**, 1017–1031 (2002)
37. H. Cho, N. Jeong, H.J. Sung, Permeability of microscale fibrous porous media using the lattice Boltzmann method. *Int. J. Heat Fluid Flow* **44**, 435–443 (2013)